JACC: BASIC TO TRANSLATIONAL SCIENCE VOL. 5, NO. 2, 2020

PRECLINICAL RESEARCH

Macrophage-Derived Exosomal Mir-155 Regulating Cardiomyocyte Pyroptosis and Hypertrophy in Uremic Cardiomyopathy

Bin Wang, MD, PhD,[a,*] Ze-Mu Wang, MD, PhD,[b,*] Jia-Ling Ji, MD,[c] Weihua Gan, PhD,[c] Aiqing Zhang, PhD,[c] Hao-Jie Shi, MD,[b] Hao Wang, PhD,[b] Linli Lv, MD,[a] Zuolin Li, MD,[a] Taotao Tang, MD,[a] Jie Du, PhD,[d] Xiaonan H. Wang, MD,[e] Bi-Cheng Liu, MD, PhD[a]

VISUAL ABSTRACT

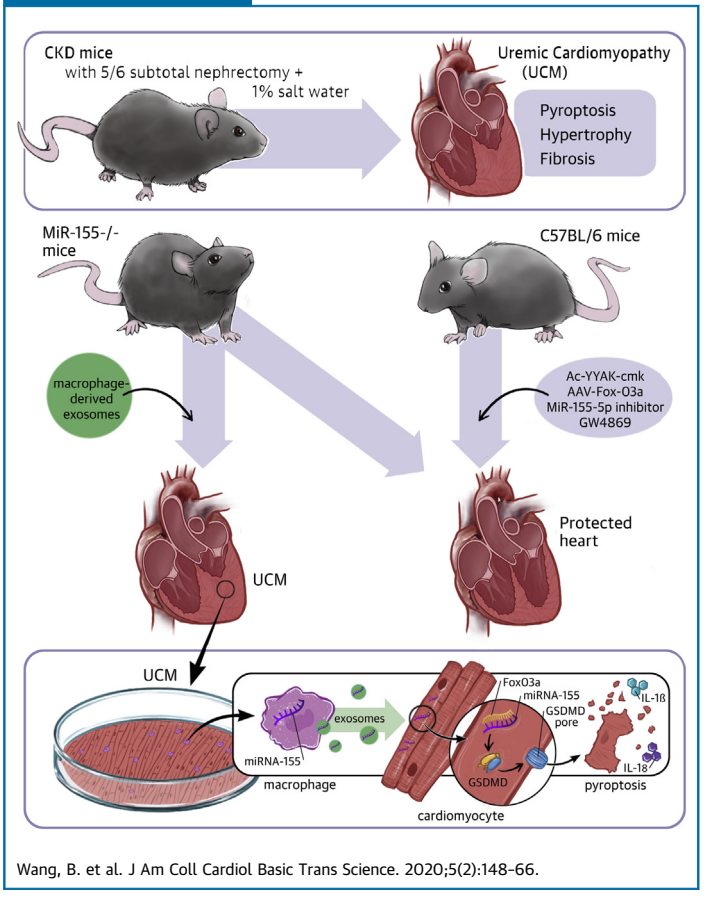

Wang, B. et al. J Am Coll Cardiol Basic Trans Science. 2020;5(2):148–66.

HIGHLIGHTS

- **miR-155 was synthesized and loaded into exosomes in increased infiltration of macrophages in a uremic heart.**
- **The released exosomal fusion with the plasma membrane leads to the release of miR-155 into the cytosol and translational repression of forkhead transcription factors of the O class in cardiomyocytes.**
- **Macrophage-derived miR-155–containing exosomes promoted cardiomyocyte pyroptosis and uremic cardiomyopathy changes (cardiac hypertrophy and fibrosis) by directly targeting FoxO3a in uremic mice. Inhibiting secretion from macrophage-derived miR-155–containing exosomes represents a novel therapeutic strategy for the management of uremic cardiomyopathy.**

From the [a]Institute of Nephrology, Zhong Da Hospital, Southeast University School of Medicine, Nanjing, Jiangsu, China; [b]Department of Cardiology, The First Affiliated Hospital of Nanjing Medical University, Nanjing, Jiangsu, China; [c]Department of Pediatric Nephrology, the Second Affiliated Hospital of Nanjing Medical University, Nanjing, Jiangsu, China; [d]Beijing Anzhen Hospital, Capital Medical University, Beijing, China; and the [e]Department of Medicine, Renal Division, Emory University, Atlanta, Georgia. *Drs. B. Wang and Z.-M. Wang contributed equally to this work and are joint first authors. This work was supported by

ISSN 2452-302X https://doi.org/10.1016/j.jacbts.2019.10.011

SUMMARY

miR-155 was synthesized and loaded into exosomes in increased infiltration of macrophages in a uremic heart. The released exosomal fusion with the plasma membrane leads to the release of miR-155 into the cytosol and translational repression of forkhead transcription factors of the O class (FoxO3a) in cardiomyocytes. Finally, macrophage-derived miR-155–containing exosomes promoted cardiomyocyte pyroptosis and uremic cardiomyopathy changes (cardiac hypertrophy and fibrosis) by directly targeting FoxO3a in uremic mice.

ABBREVIATIONS AND ACRONYMS

3'-UTRs = 3'-untranslated regions
AAV = adeno-associated virus
CKD = chronic kidney disease
FoxO = forkhead transcription factors of the O class
IL = interleukin
LV = left ventricle
miRs = microRNAs
TUNEL = deoxyuridine triphosphate nick-end labeling
UCM = uremic cardiomyopathy

Uremic cardiomyopathy (UCM) is a major complication of chronic renal failure whose treatment remains disappointing. UCM, characterized by cardiac hypertrophy, fibrosis, inflammation, and metabolic remodeling, accounts for approximately 50% of deaths due to chronic kidney disease (CKD) (1–3). It is thought that traditional cardiovascular risk factors such as hypertension, volume overload, and anemia are major causes of UCM; however, UCM may also develop independently of these above-mentioned risk factors (4,5). Although a number of factors, including metabolic acidosis, inflammation, increased oxidant stress, and insulin resistance may contribute to the development of UCM (1,6,7), the exact mechanism is still largely unknown.

SEE PAGE 167

Pyroptosis is a pro-inflammatory programmed cell death, which is mainly mediated by caspase1 activation and subsequently processes the proforms of inflammatory cytokines (interleukin [IL]-1β and IL-18) into active forms (8). Pyroptosis is morphologically and mechanistically distinct from other forms of cell death (apoptosis and necroptosis). Apoptosis is perhaps the most widely recognized program of cell death, and is initiated by caspases 2, 8, 9, and 10, and requires the effector caspases 3, 6, and 7 (9). In contrast, pyroptosis is mainly mediated by caspase 1 activation and is a programmed process of cellular self-destruction, and therefore was not initially distinguished from apoptosis (8). Pyroptosis is generally considered as cell death plus inflammation and is mediated by caspase 1 activation (6). Accumulating evidence has identified the vital role of apoptosis and inflammation in the development of UCM (10,11). However, whether pyroptosis is involved in UCM and the potential mechanism that is involved have not been clarified.

Forkhead transcription factors of the O class (FoxO1, FoxO3, FoxO4, and FoxO6) transcriptionally activate or inhibit a number of target genes and play important roles in proliferation, apoptosis, inflammation, and pyroptosis (12). In the heart, FoxO1 and FoxO3a are the dominant FoxO family members (13,14). Activation of FoxO1 and FoxO3a is an important mediator of pathologic cardiac hypertrophy (15,16). MicroRNAs (miRs) are short, noncoding RNAs that downregulate proteins by binding to complementary sequences in the 3'-untranslated regions (3'-UTRs) of target mRNAs (17). miRs have also been shown to be involved in pyroptosis through FoxO regulation: 1) Dysregulated miR-148a in hepatocytes through FoxO1 facilitate pyroptosis in alcoholic liver disease (18); and 2) miR-30d regulates cardiomyocyte pyroptosis by directly targeting FoxO3a in patients with diabetic cardiomyopathy (19). In our previous

grants from the National Natural Science Foundation of China (No 81700618), the Natural Science Foundation of Jiangsu Province (BK20181487), China Young Nephrologist Research Project, and Southeast University High Level Thesis Project to Dr. B. Wang; the National Natural Science Foundation of China (No 81703213), the Natural Science Youth Foundation of Jiangsu Province of China (No. BK20151034) to Dr. Z.-M. Wang; the National Natural Science Foundation of China (No 81470922, 31671194, 81720108007, and 81670696) , National Key Research Program (2018YFC1314000) and Clinic Research Center of Jiangsu Province (BL2014080) to Dr. B.-C. Liu. The authors have reported that they have no relationships relevant to the contents of this paper to disclose.
The authors attest they are in compliance with human studies committees and animal welfare regulations of the authors' institutions and Food and Drug Administration guidelines, including patient consent where appropriate. For more information, visit the *JACC: Basic to Translational Science* author instructions page.

Manuscript received June 3, 2019; revised manuscript received October 29, 2019, accepted October 29, 2019.

studies, we have shown that a range of miRs (e.g., miR-23a, miR-26a, miR-27a, and miR-29) could downregulate FoxO1 and/or FoxO3 expression in skeletal muscle and heart under uremic stress conditions (17,20–22). However, the role of miRs/FoxO axis in patients with UCM is largely unknown.

Mammalian cells produce miRs that not only regulate physical activity per se, but also influence neighboring cells, and even distant cells in other organs (23,24). Exosomes are small 30- to 150-nm vesicles formed within cells by inward budding of the limiting membrane of multivesicular bodies within the cytoplasm. Exosomes have been shown to be natural carriers of many signal molecules, including miRs that mediate cell-cell communication and thus play critical roles in the physiology and pathogenesis of cancer (25), autoimmune diseases (26), and cardiovascular diseases (27). It is well-known that macrophage infiltration is a common feature of cardiomyopathies, and previous studies have proven that macrophage-derived exosomes induce inflammatory factors (28,29) and cell death (30).

In the current study, our results have shown that infiltrated macrophages secrete miR-155–enriched exosomes and promote cardiomyocyte pyroptosis by directly targeting FoxO3a in a uremic mouse, thus blocking macrophage-derived miR-155–containing exosomes may be a promising therapeutic target for the management of UCM.

METHODS

ANIMALS AND UREMIC MOUSE MODEL. miR-155$^{-/-}$ mice in a C57BL/6 background were provided by Dr. Jie Du (Beijing Anzhen Hospital, Capital Medical University, Beijing, China). Wild-type male C57BL/6 mice (22 to 25 g) were purchased from The Jackson Laboratory (Bar Harbor, Maine). Under pentobarbital anesthesia, the uremic mouse model was obtained through a two-step, 5/6th nephrectomy. During the first week we removed two-thirds of the left kidney. After a 1-week recovery, we removed the right kidney. After the second surgery, all mice were fed with 1% salt water. Uremic mice with a blood urea nitrogen level of 100 mg/dl (Reflotron Plus Diagnostic Device; Roche Diagnostics Corporation, Indianapolis, Indiana) were studied.

CASPASE-1 INHIBITOR EXPERIMENT. To inhibit caspase-1 activity in vivo, mice received Ac-YVAD-cmk (8 mg/kg per time, once weekly for 8 weeks; InvivoGen, San Diego, California) in dimethyl sulfoxide (5% v/v) or dimethyl sulfoxide alone intraperitoneally.

VIRUS AND GENE DELIVERY. A type 9 recombinant adeno-associated virus (AAV)-expressing mouse FoxO3a gene with enhanced green fluorescent protein (GFP) (AAV-FoxO3a-GFP) and a recombinant AAV encoding GFP (AAV-GFP) as the control vector were purchased from Genechem Biotech, Inc. (Shanghai, China). AAVs (1×10^{11} virion particles in 100 ml saline solution) were delivered via a single tail injection after the second surgery. miR-155 inhibitor was synthesized by Genechem Biotech, Inc. In vivo-jetPEI (Polyplus Transfection, New York, New York) was used to deliver miR-155 inhibitor into the heart via tail injection (60 ng, once weekly for 8 weeks).

ECHOCARDIOGRAPHY. Echocardiography was performed on lightly anesthetized mice under 1% to 2% isoflurane in oxygen using a Vevo 3100 ultrasound system (VisualSonics, Toronto, Ontario, Canada), as described previously (31). Left ventricular (LV) dimensions were obtained from parasternal long-axis views by 2-dimensional-sided M-mode imaging, in which the cursor was positioned perpendicular to the interventricular septum and posterior wall of the LV at the level of the papillary muscles and a M-mode image was obtained at a sweep speed of 100 mm/s and used to determine diastolic and systolic LV wall thickness, LV end-diastolic dimensions (LVDDs), and LV end-systolic chamber dimensions (LVSDs). Systolic function was calculated from LV dimensions as fractional shortening (FS), as follows: $FS = (LVDD - LVSD)/LVDD$. Recording of echocardiographic images was performed in random order with respect to the treatment or control animals. The acquisition of images and evaluation of data were performed by an independent operator who was blinded to the treatment.

MORPHOLOGIC ANALYSIS AND IMMUNOHISTOCHEMISTRY. Briefly, formalin-fixed, paraffin-embedded heart sections (3-μm thick) stained with hematoxylin and eosin (HE) and Masson's trichrome stain were used to evaluate myocardial cell size and heart fibrosis, respectively. Indirect immunohistochemistry staining was performed according to an established procedure (32). After being blocked with 3% bovine serum albumin for 1 h, the sections were incubated overnight at 4°C with primary antibodies against caspase 1 (1:200) in phosphate-buffered saline (PBS) solution containing 3% bovine serum albumin. Staining was visualized using horseradish peroxidase-coupled secondary antibodies (Vectastain

Elite; Vector Labs, Burlingame, California). All immunohistochemical analyses were repeated at least 3 times and representative images are shown.

CELL ISOLATION BY FLOW SORTING. Cell isolation by flow sorting was performed as described (33). Macrophages, T cells, endothelial cells, cardiac fibroblasts, and cardiomyocytes were sorted based on CD45+CD11b+, CD45+ CD11b-, CD45-CD31+, CD45-CD31-PDGFR+, and CD45-CD31-PDGFR-, respectively.

EXOSOME PURIFICATION, ANALYSIS, AND MODIFICATION. Conditioned medium of RAW264.7 cultured in fetal bovine serum (FBS)-free Dulbecco's Modified Eagle Medium (DMEM) were collected for 48 h and exosomes were purified by several centrifugation and filtration steps, as described previously (15). Briefly, the supernatant was centrifuged at 2,000 × g for 10 min and 16,000 × g for 30 min, followed by filtration through a 0.22-μm filter to eliminate cells, dead cells, and cellular debris. For exosome purification, the supernatant was ultracentrifuged at 160,000 × g for 180 min (L8-70M ultracentrifuge; Beckman Coulter, Brea, California). The exosome pellets were re-suspended in PBS and stored at −80℃.

EXOSOME TRANSFUSION EXPERIMENT. Saline or exosomes derived from RAW264.7 (100 or 200 mg) were injected intravenously into miR-155$^{-/-}$ mice every week for a total of 8 injections. The exosomes were first injected on the second day and the following 7 injections were performed every week after the second operation. The mice were sacrificed after 10 weeks and the hearts were harvested for subsequent experiments.

TERMINAL DEOXYNUCLEOTIDYL TRANSFERASE DEOXYURIDINE TRIPHOSPHATE NICK-END LABELING STAINING. Cell death was detected using the terminal deoxynucleotidyl transferase deoxyuridine triphosphate nick-end labeling (TUNEL) assay with an in situ apoptosis detection kit (Takara Bio Inc., Tokyo, Japan). Cell death was defined as the presence of nuclear condensation via 4',6'-diamidino-2-phenylindole (DAPI) staining and TUNEL-positive cells within the heart. The proportion of cardiomyocytes with TUNEL-positive cells in formalin-fixed heart tissues was determined by examination at 400× magnification.

TRANSMISSION ELECTRON MICROSCOPY. Transmission electron microscopy was performed on purified exosomes from the cell culture medium, as previously described (32). Briefly, exosome pellets were mixed 1:1 with 4% paraformaldehyde, and then applied to 200-mesh nickel grids. Samples were left to immobilization at room temperature for 20 min. The excess solution was absorbed by filter paper and the grid was stained with 2% uranyl acetate in water for 10 s, washed 3 times in distilled water, and air-dried. Samples were examined using a Tecnai 10 TEM (Fei, Acht, the Netherlands) at 80 kV.

WESTERN BLOT ANALYSIS. Cells harvested from plates and heart tissues were lysed in radioimmunoprecipitation assay buffer. Detection of protein expression by Western blot was performed according to established protocols. Equal amounts of protein were subjected to sodium dodecyl sulfate-polyacrylamide gel electrophoresis on 10% to 12% polyacrylamide gels and transferred to a polyvinylidene difluoride membrane (HATF09025; Millipore, Bedford, Massachusetts). The membrane with blotted protein was blocked for 1 h with blocking buffer containing 5% nonfat dry milk and 0.05% Tween-20 in Tris-buffered saline (TBS-T), followed by incubation with the primary antibodies as follows: caspase 1 (Abcam, Cambridge, Massachusetts); IL-1β (Abcam); IL-18 (Santa Cruz Biotechnology, Dallas, Texas); FoxO1 (Cell Signaling Technology, Beverly, Massachusetts); FoxO3a (Cell Signaling Technology); Gsdmd (Abcam), Alix (Santa Cruz Biotechnology); CD63 (Abcam); CD9 (Abcam); CD68(Abcam); iNOS (Abcam); Tubulin (Abbkine, Beijing, China) and GAPDH (CMCTAG, Milwaukee, Wisconsin). Then, the membranes were thrice-washed with TBS-T for 30 min and incubated at room temperature for 1 h with diluted (1:10,000) secondary horseradish peroxidase-conjugated goat anti-rabbit immunoglobulin G (IgG) or goat anti-mouse IgG. The bands were detected using the ChemiDoc XRS System (Bio-Rad, Hercules, California). The relative intensity of each band was normalized to GAPDH.

REAL-TIME POLYMERASE CHAIN REACTION. For mRNA profile analysis, RNA was extracted from heart samples with Trizol (Invitrogen, Carlsbad, California), reverse-transcribed into complementary DNA (cDNA) (Taqman Reverse Transcription Reagents; Applied Biosystems-Roche, Branchburg, New Jersey), and mRNA abundance was analyzed by real-time polymerase chain reaction (PCR) with SYBR-Green (iTaq or iQ SYBR-Green Supermix, BioRad). All of the primers for quantitative real-time PCR are listed in Supplemental Table 1. Relative expression was normalized to GAPDH levels.

For miR profile analysis, RNA enriched in small RNAs was extracted from the exosomes and heart tissues using a mirVana miRNA isolation kit (Ambion, Austin, Texas). Only miRs which were detected in all samples and had a Cycle threshold (Ct) value <35, were considered for further analysis. For synthesis

FIGURE 1 **Cardiomyocytes Pyroptosis Is Involved in the Process of UCM**

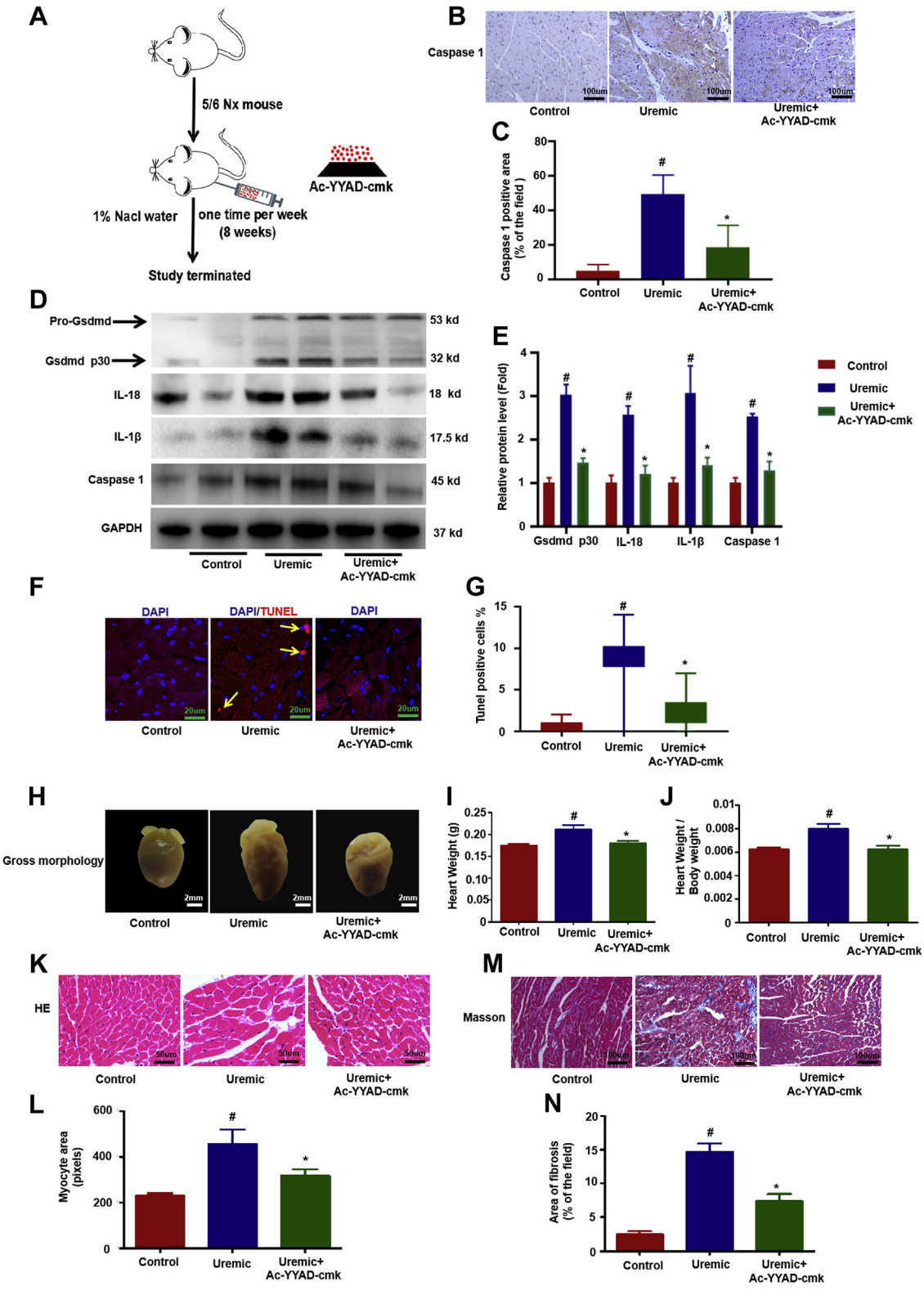

Continued on the next page

FIGURE 2 Foxo3a, But Not Foxo1, Is Downregulated in Uremic Hearts

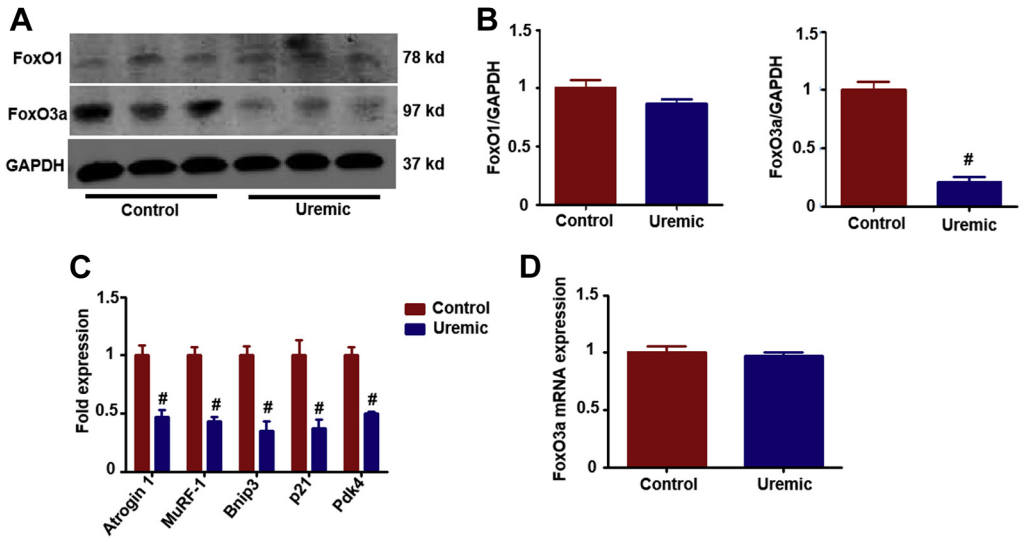

(A) Representative Western blot for Foxo1 and FoxO3a. **(B)** Bar graph showing the fold change (n = 6 per group). **(C)** The expression of FoxO-specific target genes, including Atrogin-1, MuRF-1, Bnip-3, p21, and Pdk4 (n = 6 per group). **(D)** FoxO3a mRNA levels in uremic hearts and that of the control group (n = 6 per group). #p < 0.05 versus control. FoxO3a,O1 = forkhead transcription factors of the O class.

of cDNA, 10 ng of total RNA that was enriched in small RNAs was reverse-transcribed using an NCode miRNA cDNA synthesis kit (Exiqon, Vedbaek, Denmark). The expression of pri-miR and pre-miR was measured, as previously described (34). Expression of individual miRNAs was standardized to the mouse U6 gene and calculated as the difference between the threshold values of the 2 genes ($2^{\Delta ct}$). Melting curve analyses were performed during real-time quantitative PCR to analyze and verify the specificity of the reaction.

PRIMARY CULTURE OF NEONATAL RAT CARDIOMYOCYTES. Cardiomyocytes were isolated from hearts of neonatal SD rats using established methods (35). Briefly, the ventricles were digested with collagenase (0.4 mg/ml) and pancreatin (0.6 mg/ml) in 116 mM NaCl, 20 mM HEPES (pH 7.35), 0.8 mM NaH_2PO_4, 5.6 mM glucose, 5.4 mM KCl, 0.8 mM $MgSO_4$. The supernatant was added to one-fifth (20%) volume horse serum to stop digestion and resuspended in DMEM with 10% horse serum, 5% FBS, penicillin (100 U/ml), and streptomycin (100 μg/ml). The collected supernatant was passed through a 100-μm cell strainer and plated in petri dishes for 45 min at 37°C to adhere to fibroblasts. The supernatant was centrifuged at 1,000 rpm for 5 min. Percoll-separated digests were performed to distinguish cardiomyocytes, fibroblasts, and other cells. Finally, the collected cardiomyocytes were plated on gelatin-coated plates under culture conditions (37°C in 5% CO_2) (Supplemental Figure 1).

EXOSOME-CARDIOMYOCYTES FUSION. Exosomes harvested from the medium of cultured macrophages (RAW264.7) were labeled with 2 μM PKH67

FIGURE 1 Continued

(A) Overview of the experimental in vivo procedure. **(B)** Representative immunohistochemical staining of caspase 1. **(C)** Quantification of caspase-1 expression in heart tissues (n = 6 per group). **(D)** The level of caspase-1, IL-1β, IL-18, and Gsdmd p30 protein. **(E)** Graphic presentation shows the relative abundance levels of caspase-1, IL-1β, IL-18, and Gsdmd p30 after normalization with GAPDH (n = 6 per group). **(F)** TUNEL assay; the **yellow arrows** indicate TUNEL-positive cardiomyocytes. **(G)** Quantification of TUNEL-positive cardiomyocytes (n = 6 per group). **(H)** Gross morphology of heart. **(I)** Summary of heart weight (n = 6 per group) and **(J)** heart weight/body weight (n = 6 per group). **(K)** Representative micrographs of sagittal sections (HE). **(L)** Summary of myocyte size (n = 6 per group). **(M)** Representative micrographs of left ventricular sections (Trichrome). **(N)** Summary of semiquantification of the Trichrome-positive area (n = 6 per group). Scale bars: 2 mm, **(F)**; 50 μm **(B, K, M)**. #p < 0.05 versus control, *p < 0.05 versus uremic group. DAPI = 4′,6′-diamidino-2-phenylindole; HE = hematoxylin and eosin stain; IL = interleukin; TUNEL = terminal deoxynucleotidyl transferase deoxyuridine triphosphate nick-end labeling; UCM = uremic cardiomyopathy.

FIGURE 3 Overexpression of Foxo3a Attenuated Cardiomyocytes Pyroptosis and Improved UCM

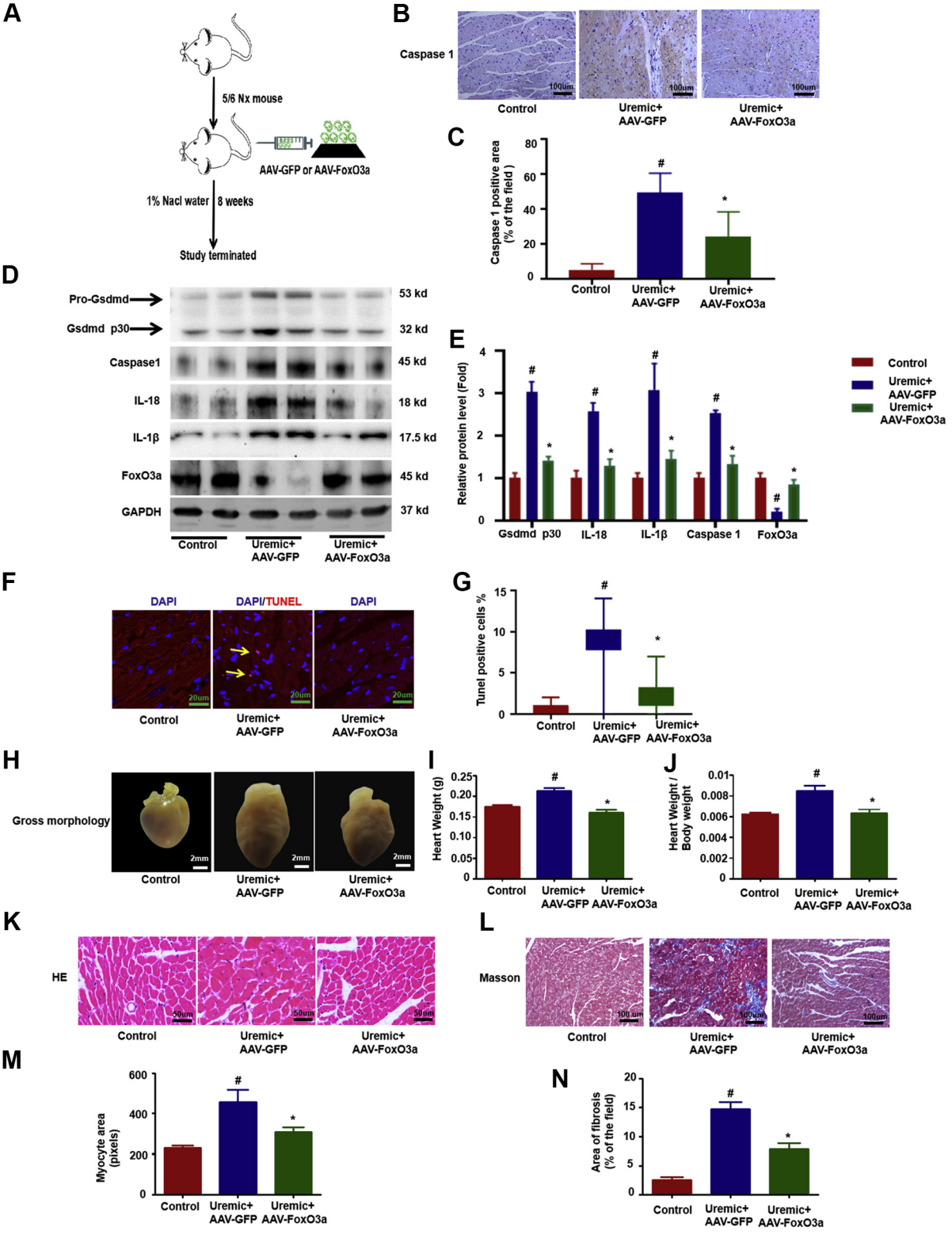

Continued on the next page

(Sigma-Aldrich, St. Louis, Missouri) for 5 min, washed and incubated for 24 h with cultured cardiomyocytes. The samples were washed and counterstained with DAPI, and analyzed by light and fluorescence microscopy.

LUCIFERASE REPORTER ASSAY AND TRANSFECTION. Effectene transfection reagent was used for transfection (Qiagen, Valencia, California) of cardiomyocytes (36). Firefly and Renilla luciferase activities were measured using a dual luciferase assay (Promega, Madison, Wisconsin) and a luminometer (Turner Designs, Sunnyvale, California). The parent luciferase reporter plasmid (pMIR-REPORT Luciferase) was purchased from Applied Biosystems (Waltham, Massachusetts) and 3'-UTR-specific constructs were prepared by the Emory Integrated Genomics Core (Atlanta, Georgia). Results from control experiments (pLuc-3'-UTR-FoxO3a-expressing cells treated with a mimic control) are expressed as 100%. Experimental results were calculated in the same fashion and expressed as a proportion of control levels.

FLOW CYTOMETRY. The cultured cardiac myocytes were washed twice and 1×10^6 cells were suspended in 50 μL of PBS supplemented with 1% FBS. The cells were stained with FLICA (FAM-VAD-FMK655; ImmunoChemistry Technologies, Bloomington, Minnesota) for 40 min at 37°C, followed by the addition of 7AAD (BD Pharmingen, San Diego, California) before loading. The stained cells were analyzed with a FACS Calibur flow cytometer and the data were analyzed using FlowJo software.

STATISTICAL ANALYSES. Data are expressed as the mean ± SEM. Comparisons between 2 groups were performed with Student's *t* test and multiple groups were compared with one-way analysis of variance followed by Dunnett's multiple comparison test. To exclude or reduce type I errors in the multiple comparisons, Bonferroni and Sidak corrections were used to adjust the p value. A p value <0.05 was considered statistically significant. Statistical analyses were performed using Prism 7.0 (GraphPad Software, San Diego, California).

RESULTS

CARDIOMYOCYTE PYROPTOSIS IS INDUCED IN UCM. First, to confirm that pyroptosis is involved in the process of UCM, we measured the levels of caspase-1, IL-1β, and IL-18, as well as programmed cell death in uremic mice in the presence or absence of caspase 1 inhibitor treatment (Ac-YYAD-cmk) (**Figure 1A**). Our results showed that caspase-1, IL-1â, and IL-18 levels were remarkably increased in the UCM group (**Figures 1B to 1E**). Another critical target of caspase-1 is the pore-forming pyroptosis perforin, Gsdmd, which is cleaved into its active form (Gsdmd p30 protein) by caspase-1 and forms pores promoting cell swelling and lytic cell death (37–39). As expected, cleaved Gsdmd p30 protein was increased in the heart of mice following uremic challenge (**Figures 1D and 1E**). Furthermore, increased cell death occurred in UCM, whereas cell death rarely occurred in the control group (**Figures 1F and 1G**); however, Ac-YYAD-cmk significantly attenuated all of these changes (**Figures 1B to 1G**). Additionally, Ac-YYAD-cmk improved UCM, as evidenced by the significantly reduced heart size (**Figure 1H**), heart weight (**Figure 1I**), ratio of heart weight-to-body weight (**Figure 1J**), myocardial hypertrophy (**Figures 1K and 1L**), and interstitial fibrosis area (**Figures 1M and 1N**) compared with uremic hearts. Echocardiography and hemodynamic measurements showed that the LV end-diastolic dimension (LVDD), LV end-systolic dimension (LVSD) and left ventricular volume in diastole and systole (LV vol-d and LV vol-s) were all significantly increased in the hearts of uremic mice. These changes were accompanied by a decrease in the ejection fraction and FS in CKD mice. Provision of Ac-YYAD-cmk improved all of these CKD-induced changes in cardiac function parameters (Supplemental Table 2). These results suggest that

FIGURE 3 Continued

AAV-FoxO3a-GFP was generated to overexpress FoxO3a in the hearts of uremic mice through a single tail injection (1 day after the second surgery). **(A)** Overview of the experimental in vivo procedure. **(B)** Representative immunohistochemical staining of caspase-1. **(C)** Quantification of caspase-1 expression in heart tissues (n = 6 per group). **(D)** Levels of Gsdmd p30, caspase-1, IL-1β, IL-18, and FoxO3a proteins. **(E)** Graphic presentation shows the relative abundance levels of Gsdmd p30, caspase-1, IL-1β, IL-18, and FoxO3a after normalization with GAPDH (n = 6 per group). **(F)** TUNEL assay; the **yellow arrows** indicate TUNEL-positive cardiomyocytes. **(G)** Quantification of TUNEL-positive cardiomyocytes (n = 6 per group). **(H)** Gross morphology of heart. **(I)** Summary of heart weight (n = 6 per group) and **(J)** heart weights/body weights (n = 6 per group). **(K)** Representative micrographs of sagittal sections (HE). **(L)** Representative micrographs of left ventricular sections (Trichrome). **(M)** Summary of myocyte size (n = 6 per group). **(N)** Summary of semi-quantification of the Trichrome-positive area (n = 6 per group). Scale bars: 2 mm **(F)**; 50 μm **(B, K, M)**. #p < 0.05 versus control, *p < 0.05 versus uremic group. AAV = adeno-associated virus; GFP = green fluorescent protein; other abbreviations as in **Figures 1 and 2**.

FIGURE 4 **Inhibiting Mir-155 Expression Attenuated Cardiomyocytes Pyroptosis and UCM by Targeting Foxo3a 3'-UTR**

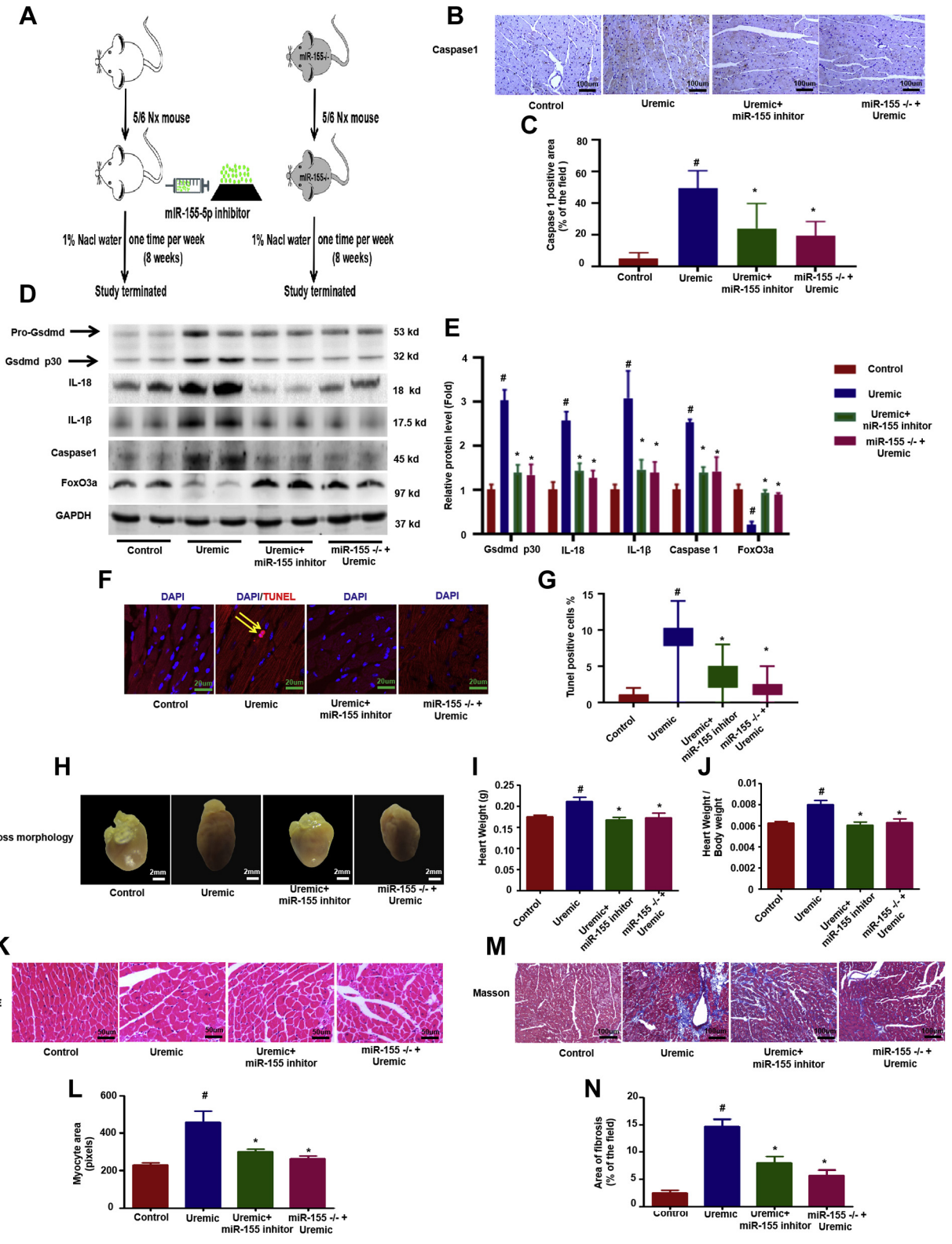

Continued on the next page

pyroptosis plays a vital role in the development of UCM.

FoxO3a, BUT NOT FoxO1, IS DOWNREGULATED IN UREMIC HEARTS. The FoxO family has been shown to be involved in regulating cardiomyocyte proliferation and cardiac growth during development and exerts a protective effect against stress resistance, inflammation, apoptosis, and pyroptosis (19,36). FoxO1 and FoxO3a have previously been reported to have a high level of expression in the heart; however, whether the FoxO family is involved in regulation of the pyroptosis process in UCM has not been examined. FoxO3a, but not FoxO1, was significantly decreased in uremic hearts compared with the control group (**Figures 2A and 2B**). To confirm inactivation of FoxO3a in uremic hearts, we evaluated transcript levels of known FoxO-specific target genes. All 5 genes tested showed a significant decrease in mRNA levels, confirming decreased FoxO activity (**Figure 2C**). There was no significant change in FoxO3a mRNA expression in the UCM group compared with the control group (**Figure 2D**).

OVEREXPRESSION OF FoxO3a ATTENUATED PYROPTOSIS AND IMPROVED UCM. To further identify the role of decreased FoxO3a in the process of regulating pyroptosis and UCM, an AAV that expresses FoxO3a and GFP (AAV-FoxO3a-GFP) was generated to overexpress FoxO3a in the hearts of uremic mice (**Figure 3A**). Expression of GFP was clearly detectable in the hearts, kidneys, and livers of mice transduced with AAV-FoxO3a-GFP (Supplemental Figure 2). Similarly, AAV-FoxO3a-GFP partially restored the expression of FoxO3a in uremic hearts (**Figures 3D and 3E**). Overexpression of FoxO3a in uremic hearts ameliorated pyroptosis (**Figures 3B to 3F**) and improved UCM, as evidenced by significantly reduced heart size (**Figure 3H**), heart weight (**Figure 3I**), ratio of heart weight-to-body weight (**Figure 3J**), myocardial hypertrophy (**Figures 3K and 3M**), and interstitial fibrosis area (**Figures 3L and 3K**), and improved cardiac function (Supplemental Table 2), indicating the decrease in FoxO3a was at least partially responsible for the pyroptosis and pathologic changes in UCM.

INHIBITING miR-155 EXPRESSION ATTENUATED PYROPTOSIS AND UCM BY TARGETING FoxO3a 3'-UTR. There was no significant differences in the FoxO3a mRNA level in UCM compared with the control group (**Figure 2D**), suggesting a post-translational regulation mechanism is responsible for the decrease of FoxO3a in UCM. Because miRs bind 3'-UTRs of target mRNAs to repress the translation process without influencing the mRNA level, we then aimed to characterize the miRs profile of UCM and evaluate 17 miRs predicted to target FoxO3a 3'-UTR. Of the above 17 miRs, miR-155 changed most and increased 7-fold (Supplemental Figure 3). Because it is known that miR-155 regulates inflammation during cardiac remodeling, we mainly focused on the effect of miR-155 on FoxO3a expression and pyroptosis in UCM. A single miR-155 binding site was predicted in the FoxO3a 3'-UTR (site: 1497-1503) (Supplemental Figure 4A). In cardiomyocytes transfected with pMIR-FoxO3a/1477-1535, the miR-155 mimic decreased luciferase activity 55% ($p < 0.05$) and mutation of the binding site prevented the response (Supplemental Figure 4B). The hairpin inhibitor of miR-155 increased luciferase activity 1.6-fold ($p < 0.05$) in cells transfected with pMIR-FoxO3a/1477-1535 (Supplemental Figure 4B).

Compared with wild-type uremic mice, knockdown of miR-155 with the specific inhibitor induced higher levels of FoxO3a under uremic stress conditions and attenuated the pyroptosis process, as evidenced by the reduced expression of caspase-1, IL-1β, and IL-18 levels and cleaved Gsdmd p30 protein (**Figures 4A to 4E**); reduced cardiomyocyte death (**Figures 4F and 4G**) and improved UCM, as indicated by significantly reduced heart size (**Figure 4H**), heart weight (**Figure 4I**), ratio of heart weight-to-body weight (**Figure 4J**), myocardial hypertrophy (**Figures 4K and 4L**), and interstitial fibrosis area (**Figures 4M and 4N**); and improved cardiac function (Supplemental Table 2). As expected, miR-155-

FIGURE 4 Continued

miR-155 inhibitor was used to treat uremic mice through weekly tail injections for 8 weeks in wild-type uremic mice and miR-155 $^{-/-}$ mice. **(A)** Overview of the experimental in vivo procedure. **(B)** Representative immunohistochemical staining of caspase-1. **(C)** Quantification of caspase-1 expression in heart tissues ($n = 6$ per group). **(D)** Levels of Gsdmd p30, caspase-1, IL-1β, IL-18, and FoxO3a proteins. **(E)** Graphic presentation shows the relative abundance levels of Gsdmd p30, caspase-1, IL-1β, IL-18, and FoxO3a after normalization with GAPDH ($n = 6$ per group). **(F)** TUNEL assay; the **yellow arrows** indicate TUNEL-positive cardiomyocytes. **(G)** Quantification of TUNEL-positive cardiomyocytes ($n = 6$ per group). **(H)** Gross morphology of heart. **(I)** Summary of heart weight ($n = 6$ per group) and **(J)** heart weights/body weights ($n = 6$ per group). **(K)** Representative micrographs of sagittal sections (HE). **(L)** Summary of myocyte size ($n = 6$ per group). **(M)** Representative micrographs of left ventricular sections (Trichrome). **(N)** Summary of semiquantification of the Trichrome-positive area ($n = 6$ per group). Scale bars: 2 mm **(F)**; 50 μm **(B, K, M)**. #$p < 0.05$ versus control, *$p < 0.05$ versus uremic group. 3'-UTR = 3'-untranslated regions; other abbreviations as in **Figures 1 and 2**.

FIGURE 5 Macrophage-Derived Exosome Transferred Mir-155 Into Cardiomyocytes and Worsened Cardiomyocytes Pyroptosis in Vivo

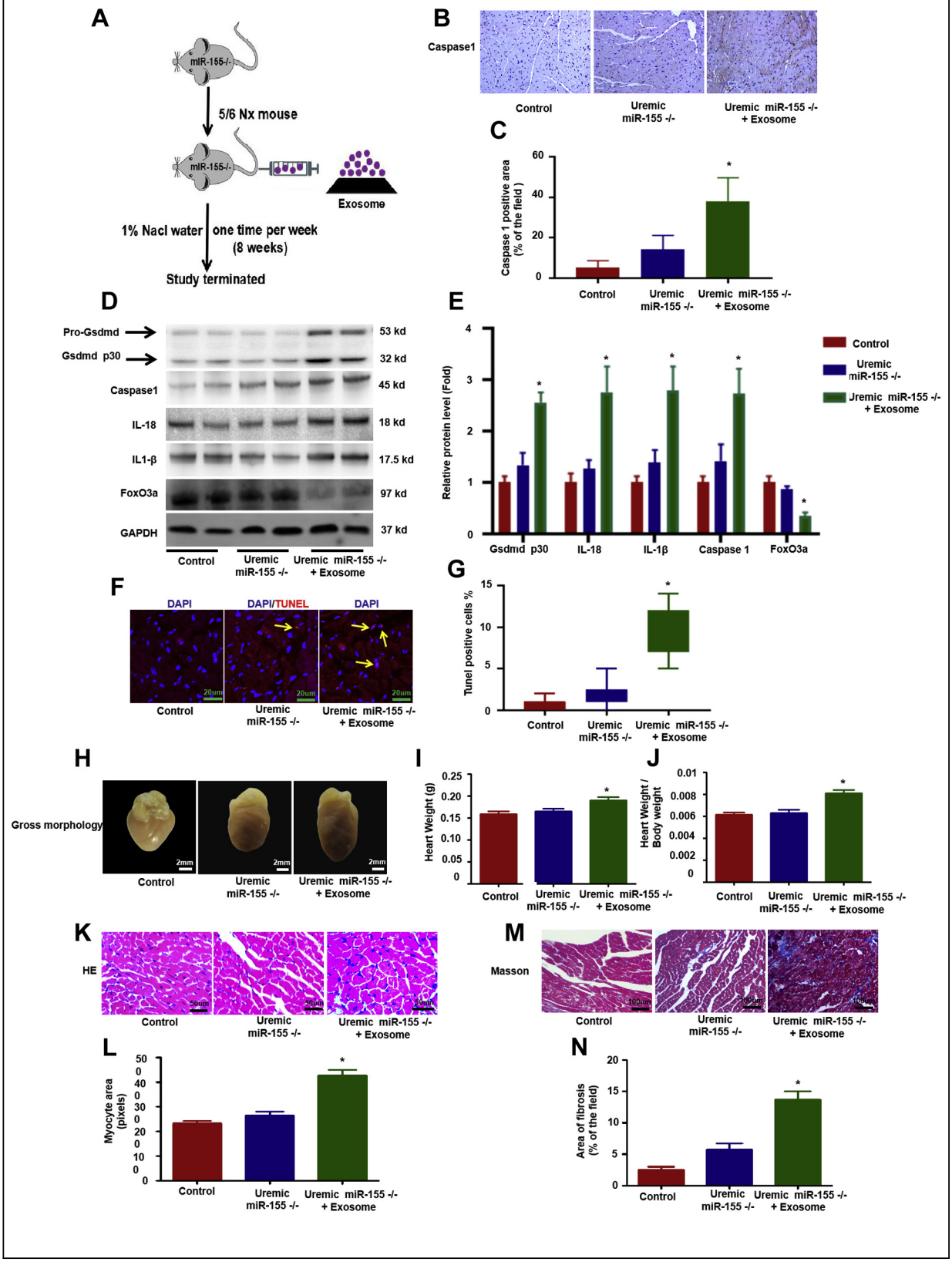

Continued on the next page

deficient mice exhibited similar results as uremic mice injected with miR-155 inhibitor (**Figure 4**, Supplemental Table 2).

MACROPHAGE-DERIVED EXOSOMES TRANSFERRED miR-155 INTO CARDIOMYOCYTES AND ENHANCED PYROPTOSIS IN VIVO. To further determine the source of miR-155 expression in uremic hearts, cardiomyocytes, cardiac fibroblasts, and macrophages were isolated from control and uremic hearts. Expression of miR-155 was the highest in macrophages, moderate in fibroblasts, and lowest in cardiomyocytes. Compared with the control group, miR-155 expression was increased in cardiomyocytes, cardiac fibroblasts, and especially infiltrated macrophages in uremic mice (Supplemental Figure 5A). pri-miR-155 was only increased in macrophages, but not in cardiomyocytes (Supplemental Figure 5B). More macrophages were infiltrated in uremic hearts as judged by the increased expression of 2 macrophage markers (iNOS and CD68) (Supplemental Figures 6A and 6B). Because miRs can be loaded into exosomes, then secreted and infused with recipient cells to mediate cell-to-cell or organ-to-organ communication, we hypothesized that miR-155 is produced in infiltrated macrophages and can be transferred into cardiomyocytes. To verify our hypothesis, we injected macrophage-derived exosomes into uremic miR-155$^{-/-}$ mice (**Figure 5A**). Macrophage-derived exosomal miR-155 enhanced pyroptosis and worsened the morphologic and functional changes in the heart of miR-155$^{-/-}$ mice under uremic stress conditions (**Figures 5B to 5N**, Supplemental Table 2).

MACROPHAGE-DERIVED EXOSOMES TRANSFERRED miR-155 INTO CARDIOMYOCYTES AND WORSENED PYROPTOSIS IN VITRO. To confirm the above findings in vitro, PKH67-labeled exosomes (**Figure 6A**), verified by transmission electron microscopy to have a size ranging from 80 to 130 nm (**Figure 6B**) and by Western blot experiments for detecting exosome markers such as Alix, CD9, and CD63 (**Figure 6C**), were transferred into primary cardiomyocytes (**Figure 6D**). Furthermore, it was found that there was a significant increase in the expression of miR-155 (**Figure 6E**) in cardiomyocytes. To further clarify whether macrophage-derived exosomes increase cardiomyocyte pyroptosis through transfer of miR-155, we stimulated primary neonatal rat cardiomyocytes with medium containing 5% uremic serum from uremic patients to mimic uremic stress conditions in the presence or absence of macrophage-derived exosomes. Macrophage-derived exosomes clearly increased pyroptosis in cardiomyocytes, as evidenced by the increased expression of caspase-1, IL-1β, IL18, and cleaved Gsdmd p30 protein, as well as an increased number of caspase-1 and propidium iodide (PI) double-positive cells in flow cytometry experiments compared with cardiomyocytes treated with 5% uremic serum alone; however, all of the changes were attenuated by treatment with miR-155 inhibitor, suggesting that macrophage-derived exosomes mediated the myocardial pyroptosis through transfer of miR-155 into cardiomyocytes (**Figures 6F through 6H**).

BLOCKADE OF EXOSOME SECRETION WITH GW4869 IMPROVES PYROPTOSIS AND UCM. GW4869, a neutral sphingomyelinase inhibitor, is the most widely used pharmacologic agent for blocking exosome generation (40,41). To further determine whether the transfer of exosomal miR-155 from macrophages into cardiomyocytes is critical for UCM (**Figure 7A**), we measured the level of miR-155 expression in isolated cardiomyocytes, cardiac fibroblasts, and macrophages in uremic hearts with or without the treatment of GW4869. GW4869 significantly decreased miR-155 levels by 37% in cardiomyocytes and 47% in cardiac fibroblasts, but profoundly increased miR-155 levels by 155% in macrophages compared with levels collected from uremic mice (Supplemental Figure 7). Furthermore, treatment with GW4869 resulted in a significant decrease in pyroptosis, as evidenced by a reduction of caspase-1, IL-18, IL-1β, and cleaved Gsdmd p30 protein (**Figures 7B to 7E**) and by a decrease in cell death (**Figures 7F and 7G**) compared with the uremic group. More impressively, we found that UCM

FIGURE 5 Continued

Uremic miR-155$^{-/-}$ mice were injected with macrophage original exosomes through weekly tail injections for 8 weeks. **(A)** Overview of the experimental in vivo procedure. **(B)** Representative immunohistochemical staining of caspase-1. **(C)** Quantification of caspase-1 expression in heart tissues (n = 6 per group). **(D)** Levels of Gsdmd p30, caspase-1, IL-1β, IL-18, and FoxO3a proteins. **(E)** Graphic presentation shows the relative abundance levels of Gsdmd p30, caspase-1, IL-1β, IL-18, and FoxO3a after normalization with GAPDH (n = 6 per group). **(F)** TUNEL assay; the **yellow arrows** indicate TUNEL-positive cardiomyocytes. **(G)** Quantification of TUNEL-positive cardiomyocytes (n = 6 per group). **(H)** Gross morphology of heart. **(I)** Summary of heart weight (n = 6 per group) and **(J)** heart weights/body weights (n = 6 per group). **(K)** Representative micrographs of sagittal sections (HE). **(L)** Summary of myocyte size (n = 6 per group). **(M)** Representative micrographs of left ventricular sections (Trichrome). **(N)** Summary of semiquantification of the Trichrome-positive area (n = 6 per group). Scale bars: 2 mm **(F)**; 50 μm **(B, K, M)**. #$p < 0.05$ versus control, *$p < 0.05$ versus uremic group. Abbreviations as in **Figures 1 and 2**.

FIGURE 6 **Macrophage-Derived Exosome Transfer of Mir-155 Into Cardiomyocytes and Worsened Pyroptosis in Vitro**

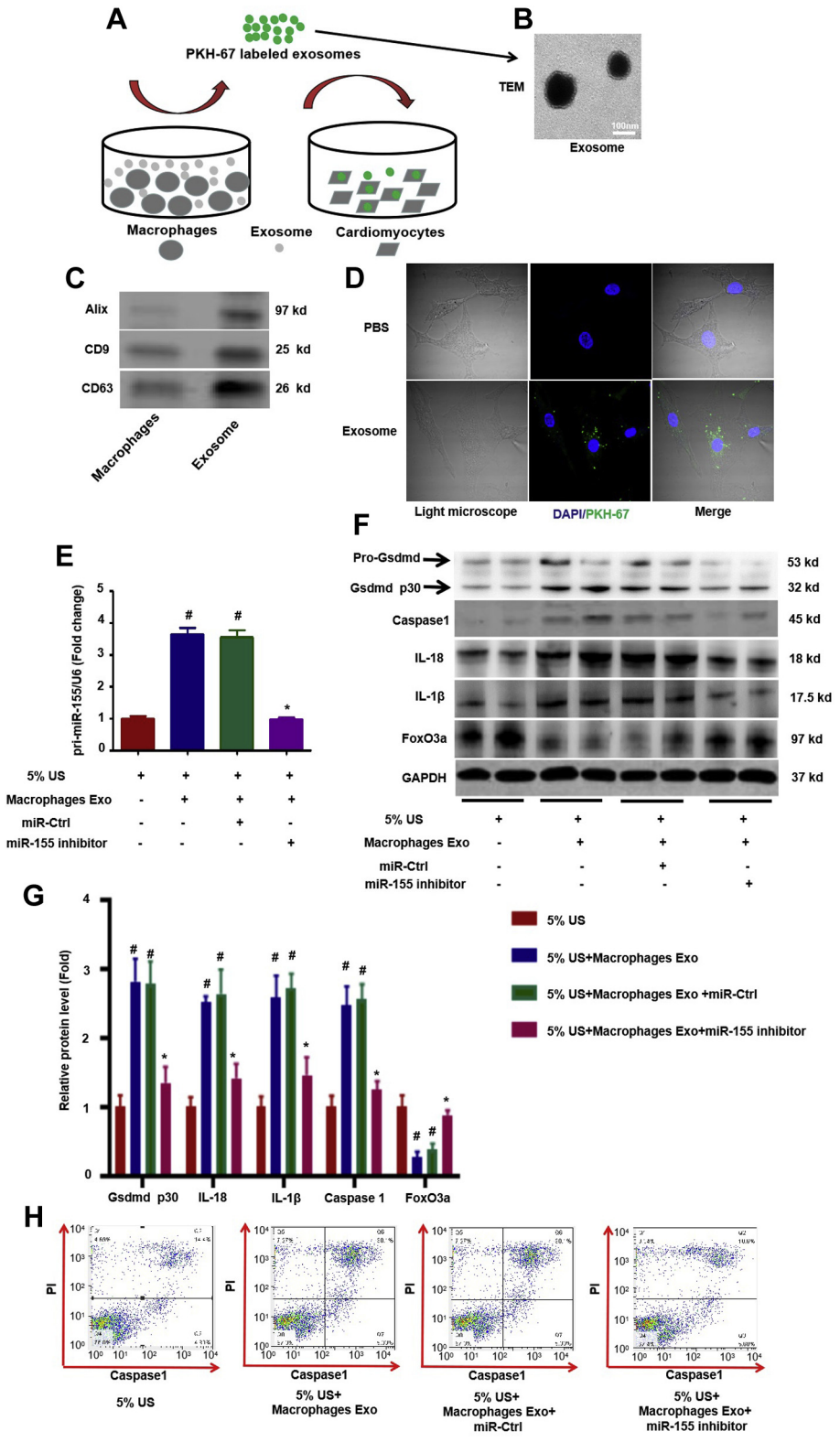

Continued on the next page

was clearly improved with GW4869 upon uremic challenge compared to the control (**Figures 7H to 7N**). Taken together, our results suggested that pyroptosis of myocardiocytes in uremia was mediated by the exosomes derived from macrophages.

DISCUSSION

In the present study, we first showed that exosomal miR-155 derived from macrophages is critical in mediating cardiomyocyte pyroptosis in uremic hearts by downregulating FoxO3a protein expression, as summarized in **Figure 8**. These findings provide novel insight about uremic heart disease and may indicate a new therapeutic target for this life-threatening disorder.

UCM is a widely prevalent cardiovascular disease in patients with end-stage renal disease and more than 50% of dialysis patients died of cardiovascular disease. Cardiac hypertrophy, 1 of the most key features of UCM, is seen in approximately 75% of adult patients at the onset of dialysis, and almost 100% of patients after 5 years on dialysis (42–44). Understanding the molecular mechanism will contribute to the development of clinical intervention strategies to UCM. The FoxO family of transcription factors play a key role in a number of cellular processes, including cell growth, metabolism, and survival (15,45,46). In murine hearts, FoxO3a overexpression inhibits cardiac hypertrophy (47). Whether FoxO-dependent signaling plays a role in UCM has not been determined. Here, our results for the first time showed that decreasing FoxO3a signaling might be responsible for the UCM changes.

Emerging evidence also suggested that inflammation and cardiomyocyte apoptosis play critical roles in the development of UCM (1,48,49). Recently, necroptosis was also proposed as a mechanism for cardiomyocyte injury under ischemia and oxidative stress condition, both of which are common stress states in UCM (50). Apoptosis is usually evidenced by detecting apoptotic markers (e.g., TUNEL and cleaved caspase-3). However, apoptosis markers are now recognized to be nonspecific. It has been shown that TUNEL-labeled cells undergo both necroptosis and proptosis, and that cleaved caspase-3 activates pyroptosis rather than apoptosis through the related protein, gasdermin E (51). In this study, we showed that pyroptosis in cardiomyocytes was markedly increased following uremic challenge both in vivo and in vitro. These findings raise the possibility that cardiomyocyte death previously attributed to apoptosis in UCM might alternatively represent pyroptosis. More important, inhibiting pyroptosis with caspase 1 inhibitor also improved cardiac hypertrophy and fibrosis, suggesting pyroptosis could be served as a potential intervention target in UCM. In the current study, overexpression of FoxO3a in the heart of uremic mice showed less pyroptosis, which is consistent with a previous study that FoxO3a negatively regulated cardiomyocyte pyroptosis through apoptosis repressor with caspase recruitment domain/caspase-1/IL-1β signaling under hyperglycemic conditions (19).

miRs are small noncoding RNAs that bind 3'-UTRs of target mRNAs to repress the translation process without influencing the mRNA level (20). In our study, knockdown of miR-155 with specific inhibitor or miR-155-deficient mice showed that FoxO3a levels were partially restored and attenuated cardiomyocyte pyroptosis, hypertrophy, and fibrosis in uremic mice. Consistently, it has been reported that miR-155 knockout mice protect the heart from pathologic cardiac hypertrophy (52). The aforementioned results suggest an important positive role for the miR-155/FoxO3a axis inducing pyroptosis in UCM.

miRs are processed from hairpin-containing primary transcripts (53). miR-155 is encoded and co-expressed from the noncoding RNA gene, BIC, and is highly expressed in macrophages (54). MiR-155 has been reported to be expressed in atherosclerotic plaques and proinflammatory macrophages in the cardiovascular system (34). In the present study, our

FIGURE 6 Continued

(A) Exosomes harvested from the medium of cultured macrophages (RAW264.7) were labeled with PKH67 and added to primary cardiomyocytes for 24 h. **(B)** Macrophage original exosome was verified by transmission electron microscopy, ranging in size from 80 to 130 nm. **(C)** Western blot for Alix, CD9, and CD63 exosome markers. **(D)** PKH67 labeled exosomes introduced into primary cardiomyocytes. **(E)** qRT-PCR analysis of miR-155 relative folds to U6 expression is shown (n = 3 per group). **(F)** Levels of Gsdmd p30, Caspase 1, IL-1β, IL-18, and FoxO3a protein. **(G)** Graphic presentation shows the relative abundance levels of Gsdmd p30, caspase-1, IL-1β, IL-18, and FoxO3a after normalization with GAPDH (n = 3 per group). **(H)** Pyroptosis, as evidenced by caspase-1 and PI double-positive cells in flow cytometry experiments in cardiomyocytes treated with macrophage-derived exosomes in the presence or absence of miR-155 inhibitor (n = 3 per group). Scale bars: 100 nm **(B)**. #$p < 0.05$ versus 5% US, *$p < 0.05$ versus 5% US plus macrophage exosome. PI = propidium iodide; qRT-PCR = quantitative real-time polymerase chain reaction; US = uremia serum; other abbreviations as in **Figures 1 and 2**.

FIGURE 7 Blockade of Exosome Secretion With GW4869 Improves Cardiomyocytes Pyroptosis and UCM

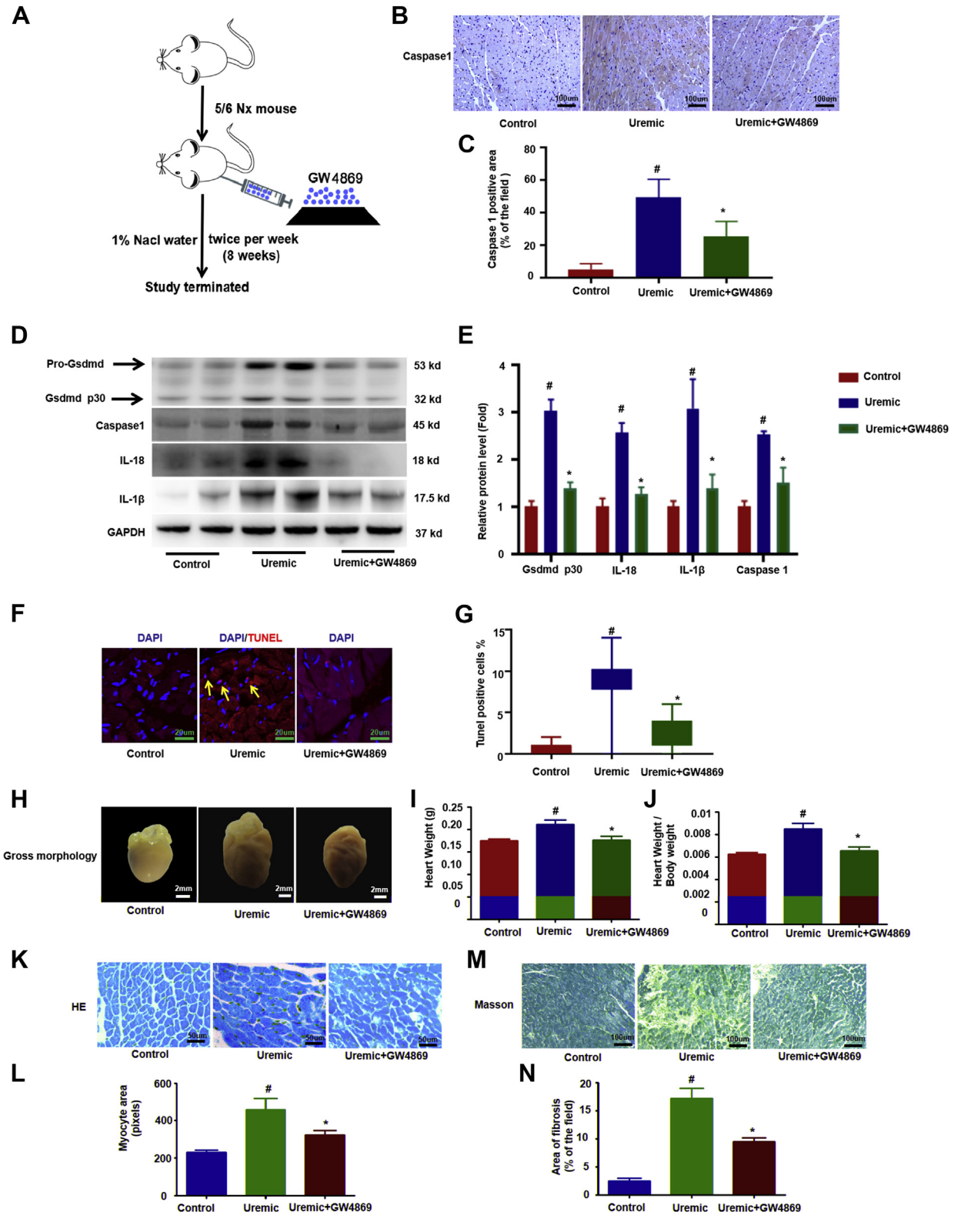

Continued on the next page

FIGURE 8 Working Model of Macrophage-Derived Mir-155–Containing Exosomes Promote Cardiomyocyte Pyroptosis by Directly Targeting Foxo3a in UCM

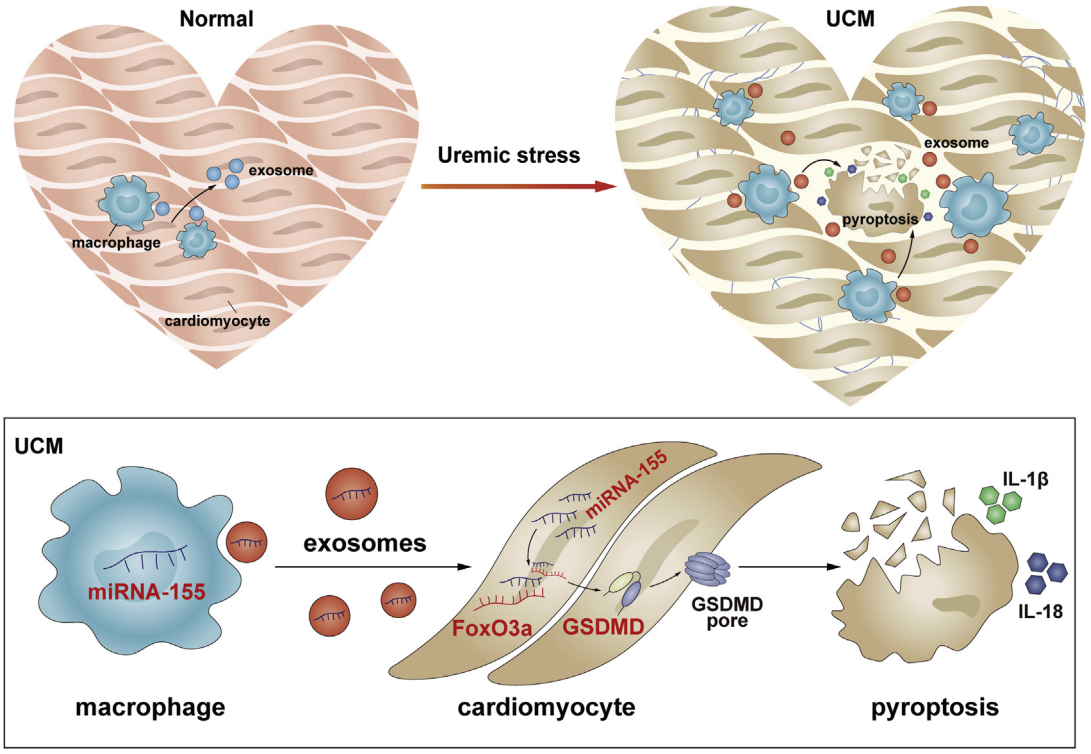

miR-155 was synthesized and loaded into exosomes in increased infiltration of macrophages in uremic heart. The released exosomal fusion with the plasma membrane leads to the release of miR-155 into the cytosol and translational repression of FoxO3a in cardiomyocytes. Finally, macrophage-derived miR-155–containing exosomes promoted cardiomyocyte pyroptosis and UCM changes (cardiac hypertrophy and fibrosis) by directly targeting FoxO3a in uremic mice. Abbreviations as in Figures 1 and 2.

results suggest that the increase of miR-155 within cardiomyocytes is originally from infiltrated macrophages. A previous study has shown that removal of miR-155 in macrophages reduces cardiac hypertrophy and cardiac dysfunction following pressure overload (55). Our results suggested that macrophage-derived miR-155 might be 1 of the key mechanisms of cardiac hypertrophy and pyroptosis in uremic cardiomyopathy. How the macrophage-derived miR-155 enters cardiomyocytes to regulate pyroptosis and hypertrophy in UCM changes is an interesting question to us.

Exosomes are nanosized membrane macrovesicles that have the capability to mediate cell-to-cell communication through transporting cell components (i.e., miRNA, mRNA, proteins, and DNA). Recent studies have shown that exosomes released from macrophages could be taken up locally by cardiomyocytes, fibroblasts, endothelial cells, and other organs (33,56). Increasing infiltration of macrophages

FIGURE 7 Continued

(A) Uremic mice were injected with GW4869 to block exosome secretion. Overview of the experimental in vivo procedure. **(B)** Representative immunohistochemical staining of caspase 1. **(C)** Quantification of caspase-1 expression in heart tissues (n = 6 per group). **(D)** Levels of Gsdmd p30, caspase-1, IL-1β, and IL-18 proteins. **(E)** Graphic presentation shows the relative abundance levels of caspase-1, IL-1β, IL-18, and Gsdmd p30 after normalization with GAPDH (n = 6 per group). **(F)** TUNEL assay; the **yellow arrows** indicate TUNEL-positive cardiomyocytes. **(G)** Quantification of TUNEL-positive cardiomyocytes (n = 6 per group). **(H)** Gross morphology of heart. **(I)** Summary of heart weight (n = 6 per group) and **(J)** heart weights/body weights (n = 6 per group). **(K)** Representative micrographs of sagittal sections (HE). **(L)** Summary of myocyte size (n = 6 per group). **(M)** Representative micrographs of left ventricular sections (Trichrome). **(N)** Summary of semiquantification of the Trichrome-positive area (n = 6 per group). Scale bars: 2 mm **(F)**; 50 μm **(B, K, M)**. #$p < 0.05$ versus control, *$p < 0.05$ versus uremic group. Abbreviations as in Figures 1 and 2.

is a typical feature of uremic hearts; however, the exact role of macrophages in uremic hearts is still not clear. In general, macrophages represent a major reservoir of cytokines and inflammatory signals controlling cardiomyocyte hypertrophy, survival, and contractility. IL-1β and IL-18 released by inflammatory macrophages enhance cardiomyocyte hypertrophy and exacerbates cardiac dysfunction as well as fibrosis in infarcted and non-infarcted heart. (57,58). In our study, blockade of exosome secretion with GW4869 attenuated pyroptosis and improved UCM in wild-type mice. Although inhibiting secretion of exosomes with GW4869 in general was not macrophage-specific or miR155-specific, GW4869 did show the improvement in UCM and cardiomyocytes pyroptosis in vivo. This result is consistent with a previous study which showed that blockade of exosome generation with GW4869 dampens the sepsis-induced inflammation and cardiac dysfunction (41). Furthermore, macrophage-derived miR-155-containing exosomes increased pyroptosis in an miR-155-dependent manner in cultured cardiomyocytes stimulated with uremic serum and worsened pyroptosis and UCM in miR-155$^{-/-}$ mice. These findings prompted us to propose a new mechanism leading to cardiomyocyte pyroptosis and hypertrophy under uremic conditions involving the transfer of exosomal miR-155 from macrophages to cardiomyocytes. Therefore, in the case of uremic cardiomyopathy, macrophages not only affect myocardial remodeling and inflammation by secreting cytokines and initiating inflammatory signals themselves, but also can amplify inflammatory reactions and affect myocardial remodeling by promoting the pyroptosis of myocardium through the transfer of miR-155-containing exosomes. For translational outlook, this new preclinical study showed a unique set of finds that are conceivably useful to inhibiting secretion from macrophage-derived miR-155-containing exosomes represents a novel therapeutic strategy for the management of UCM.

In summary, our study is the first to show that pyroptosis is involved in the pathogenesis of UCM. The striking finding of this study was the proof of concept that infiltrated macrophages secreted miR-155-enriched exosomes and promoted cardiomyocyte pyroptosis by directly targeting FoxO3a in UCM.

ACKNOWLEDGMENTS The authors thank Dr. Jie Du from Capital Medical University for providing miR-155$^{-/-}$mice.

ADDRESS FOR CORRESPONDENCE: Dr. Bi-Cheng Liu, Institute of Nephrology, Zhongda Hospital, Southeast University School of Medicine No. 87, Dingjiaqiao Road, Gulou District, Nanjing, Jiangsu Province, China. E-mail: liubc64@163.com.

PERSPECTIVES

COMPETENCY IN MEDICAL KNOWLEDGE: Animal studies have shown that both apoptosis and inflammation is involved in the development of UCM. This study raises the possibility that cardiomyocyte death previously attributed to apoptosis in UCM might alternatively represent pyroptosis. Macrophages not only affect myocardial remodeling and inflammation by secreting cytokines and initiating inflammatory signals themselves, but also can amplify inflammatory reactions and affect myocardial remodeling by promoting the pyroptosis of myocardium through the transfer of miR-155–containing exosomes in UCM.

TRANSLATIONAL OUTLOOK: Either inhibiting miR-155 directly or blocking secretion from macrophage-derived miR-155-containing exosomes represent a novel therapeutic strategy for the management of UCM.

REFERENCES

1. Semple D, Smith K, Bhandari S, Seymour AM. Uremic cardiomyopathy and insulin resistance: a critical role for akt? J Am Soc Nephrol 2011;22:207–15.

2. Hu MC, Shi M, Gillings N, et al. Recombinant α-Klotho may be prophylactic and therapeutic for acute to chronic kidney disease progression and uremic cardiomyopathy. Kidney Int 2017;91:1104–14.

3. Patient mortality and survival. United States Renal Data System. Am J Kidney Dis 1998;32:S69–80.

4. Lekawanvijit S. Cardiotoxicity of uremic toxins: a driver of cardiorenal syndrome. Toxins (Basel) 2018;10. pii:E352.

5. Alhaj E, Alhaj N, Rahman I, Niazi TO, Berkowitz R, Klapholz M. Uremic cardiomyopathy: an underdiagnosed disease. Congest Heart Fail 2013;19:E40–5.

6. Parfrey PS, Foley RN. The clinical epidemiology of cardiac disease in chronic renal failure. J Am Soc Nephrol 1999;10:1606–15.

7. El-Shehaby AM, Zakaria A, El-Khatib M, Mostafa N. Association of fetuin-A and cardiac calcification and inflammation levels in hemodialysis patients. Scand J Clin Lab Invest 2010;70:575–82.

8. Bergsbaken T, Fink SL, Cookson BT. Pyroptosis: host cell death and inflammation. Nat Rev Microbiol 2009;7:99–109.

9. Linkermann A, Chen G, Dong G, Kunzendorf U, Krautwald S, Dong Z. Regulated cell death in AKI. J Am Soc Nephrol 2014;25:2689–701.

10. McMahon AC, Naqvi RU, Hurst MJ, Raine AE, MacLeod KT. Diastolic dysfunction and abnormality of the Na+/Ca2+ exchanger in single

uremic cardiac myocytes. Kidney Int 2006;69:846–51.

11. Chin LH, Hsu YJ, Hsu SC, et al. The regulation of NLRP3 inflammasome expression during the development of cardiac contractile dysfunction in chronic kidney disease. Oncotarget 2017;8:113303–17.

12. Chaanine AH, Kohlbrenner E, Gamb SI, et al. FOXO3a regulates BNIP3 and modulates mitochondrial calcium, dynamics, and function in cardiac stress. Am J Physiol Heart Circ Physiol 2016;311:H1540–59.

13. Sengupta A, Kalinichenko VV, Yutzey KE. FoxO1 and FoxM1 transcription factors have antagonistic functions in neonatal cardiomyocyte cell-cycle withdrawal and IGF1 gene regulation. Circ Res 2013;112:267–77.

14. Philip-Couderc P, Tavares NI, Roatti A, Lerch R, Montessuit C, Baertschi AJ. Forkhead transcription factors coordinate expression of myocardial KATP channel subunits and energy metabolism. Circ Res 2008;102:e20–35.

15. Battiprolu PK, Hojayev B, Jiang N, et al. Metabolic stress-induced activation of FoxO1 triggers diabetic cardiomyopathy in mice. J Clin Invest 2012;122:1109–18.

16. Chaanine AH, Jeong D, Liang L, et al. JNK modulates FOXO3a for the expression of the mitochondrial death and mitophagy marker BNIP3 in pathological hypertrophy and in heart failure. Cell Death Dis 2012;3:265.

17. Wang B, Zhang C, Zhang A, Cai H, Price SR, Wang XH. MicroRNA-23a and microRNA-27a mimic exercise by ameliorating CKD-induced muscle atrophy. J Am Soc Nephrol 2017;28:2631–40.

18. Heo MJ, Kim TH, You JS, Blaya D, Sancho-Bru P, Kim SG. Alcohol dysregulates miR-148a in hepatocytes through FoxO1, facilitating pyroptosis via TXNIP overexpression. Gut 2019;68:708–20.

19. Li X, Du N, Zhang Q, et al. MicroRNA-30d regulates cardiomyocyte pyroptosis by directly targeting foxo3a in diabetic cardiomyopathy. Cell Death Dis 2014;5:e1479.

20. Zhang A, Li M, Wang B, Klein JD, Price SR, Wang XH. miRNA-23a/27a attenuates muscle atrophy and renal fibrosis through muscle-kidney crosstalk. J Cachexia Sarcopenia Muscle 2018;9:755–70.

21. Wang XH, Hu Z, Klein JD, Zhang L, Fang F, Mitch WE. Decreased miR-29 suppresses myogenesis in CKD. J Am Soc Nephrol 2011;22:2068–76.

22. Wang B, Zhang A, Wang H, et al. miR-26a limits muscle wasting and cardiac fibrosis through exosome-mediated microRNA transfer in chronic kidney disease. Theranostics 2019;9:1864–77.

23. Alexander M, Hu R, Runtsch MC, et al. Exosome-delivered microRNAs modulate the inflammatory response to endotoxin. Nat Commun 2015;6:7321.

24. Khan M, Nickoloff E, Abramova T, et al. Embryonic stem cell-derived exosomes promote endogenous repair mechanisms and enhance cardiac function following myocardial infarction. Circ Res 2015;117:52–64.

25. Roccaro AM, Sacco A, Maiso P, et al. BM mesenchymal stromal cell-derived exosomes facilitate multiple myeloma progression. J Clin Invest 2013;123:1542–55.

26. Perez-Hernandez J, Forner MJ, Pinto C, Chaves FJ, Cortes R, Redon J. Increased urinary exosomal microRNAs in patients with systemic lupus erythematosus. PLoS One 2015;10:e0138618.

27. Bang C, Batkai S, Dangwal S, et al. Cardiac fibroblast-derived microRNA passenger strand-enriched exosomes mediate cardiomyocyte hypertrophy. J Clin Invest 2014;124:2136–46.

28. Holder B, Jones T, Sancho Shimizu V, et al. Macrophage exosomes induce placental inflammatory cytokines: a novel mode of maternal-placental messaging. Traffic 2016;17:168–78.

29. Osada-Oka M, Shiota M, Izumi Y, et al. Macrophage-derived exosomes induce inflammatory factors in endothelial cells under hypertensive conditions. Hypertens Res 2017;40:353–60.

30. Jiao Y, Li Z, Loughran PA, et al. Frontline science: macrophage-derived exosomes promote neutrophil necroptosis following hemorrhagic shock. J Leukoc Biol 2018;103:175–83.

31. Naqvi N, Li M, Calvert JW, et al. A proliferative burst during preadolescence establishes the final cardiomyocyte number. Cell 2014;157:795–807.

32. Lv LL, Feng Y, Wen Y, et al. Exosomal CCL2 from tubular epithelial cells is critical for albumin-induced tubulointerstitial inflammation. J Am Soc Nephrol 2018;29:919–35.

33. Wang C, Zhang C, Liu L, et al. Macrophage-derived mir-155-containing exosomes suppress fibroblast proliferation and promote fibroblast inflammation during cardiac injury. Mol Ther 2017;25:192–204.

34. Nazari-Jahantigh M, Wei Y, Noels H, et al. MicroRNA-155 promotes atherosclerosis by repressing Bcl6 in macrophages. J Clin Invest 2012;122:4190–202.

35. Watkins, Borthwick, Arthur. The H9C2 cell line and primary neonatal cardiomyocyte cells show similar hypertrophic responses in vitro. In Vitro Cell Dev Biol Anim 2011;47:125–31.

36. Wu H, Huang T, Ying L, et al. MiR-155 is involved in renal ischemia-reperfusion injury via direct targeting of FoxO3a and regulating renal tubular cell pyroptosis. Cell Physiol Biochem 2016;40:1692–705.

37. He WT, Wan H, Hu L, et al. Gasdermin D is an executor of pyroptosis and required for interleukin-1β secretion. Cell Res 2015;25:1285–98.

38. Shi J, Zhao Y, Wang K, et al. Cleavage of GSDMD by inflammatory caspases determines pyroptotic cell death. Nature 2015;526:660–5.

39. Chen X, He WT, Hu L, et al. Pyroptosis is driven by non-selective gasdermin-D pore and its morphology is different from MLKL channel-mediated necroptosis. Cell Res 2016;26:1007–20.

40. Li J, Liu K, Liu Y, et al. Exosomes mediate the cell-to-cell transmission of IFN-α–induced antiviral activity. Nat Immunol 2013;14:793–803.

41. Essandoh K, Yang L, Wang X, et al. Blockade of exosome generation with GW4869 dampens the sepsis-induced inflammation and cardiac dysfunction. Biochim Biophys Acta 2015;1852:2362–71.

42. Foley RN, Parfrey PS, Harnett JD, et al. Clinical and echocardiographic disease in patients starting end-stage renal disease therapy. Kidney Int 1995;47:186–92.

43. Foley RN, Parfrey PS, Kent GM, Harnett JD, Murray DC, Barre PE. Serial change in echocardiographic parameters and cardiac failure in end-stage renal disease. J Am Soc Nephrol 2000;11:912–6.

44. Zoccali C, Benedetto FA, Mallamaci F, et al. Left ventricular mass monitoring in the follow-up of dialysis patients: prognostic value of left ventricular hypertrophy progression. Kidney Int 2004;65:1492–8.

45. Ferdous A, Battiprolu PK, Ni YG, Rothermel BA, Hill JA. FoxO, autophagy, and cardiac remodeling. J Cardiovasc Transl Res 2010;3:355–64.

46. Ronnebaum SM, Patterson C. The FoxO family in cardiac function and dysfunction. Annu Rev Physiol 2010;72:81–94.

47. Skurk C, Izumiya Y, Maatz H, et al. The FOXO3a transcription factor regulates cardiac myocyte size downstream of AKT signaling. J Biol Chem 2005;280:20814–23.

48. Jonassen AK, Brar BK, Mjøs OD, Sack MN, Latchman DS, Yellon DM. Insulin administered at reoxygenation exerts a cardioprotective effect in myocytes by a possible anti-apoptotic mechanism. J Mol Cell Cardiol 2000;32:757–64.

49. Jonassen AK, Sack MN, Mjøs OD, Yellon DM. Myocardial protection by insulin at reperfusion requires early administration and is mediated via Akt and p70s6 kinase cell-survival signaling. Circ Res 2001;89:1191–8.

50. Jin JK, Blackwood EA, Azizi K, et al. ATF6 decreases myocardial ischemia/reperfusion damage and links ER stress and oxidative stress signaling pathways in the heart. Circ Res 2017;120:862–75.

51. McKenzie BA, Mamik MK, Saito LB, et al. Caspase-1 inhibition prevents glial inflammasome activation and pyroptosis in models of multiple sclerosis. Proc Natl Acad Sci U S A 2018;115:E6065–74.

52. Seok HY, Chen J, Kataoka M, et al. Loss of microRNA-155 protects the heart from pathological cardiac hypertrophy. Circ Res 2014;114:1585–95.

53. Adams L. Non-coding RNA: pri-miRNA processing: structure is key. Nat Rev Genet 2017;18:145.

54. Tili E, Croce CM, Michaille JJ. miR-155: on the crosstalk between inflammation and cancer. Int Rev Immunol 2009;28:264–84.

55. Heymans S, Corsten MF, Verhesen W, et al. Macrophage microRNA-155 promotes cardiac hypertrophy and failure. Circulation 2013;128:1420–32.

56. Zheng B, Yin WN, Suzuki T, et al. Exosome-mediated miR-155 transfer from smooth muscle cells to endothelial cells induces endothelial injury and promotes atherosclerosis. Mol Ther 2017;25:1279–94.

57. Epelman S, Lavine KJ, Beaudin AE, et al. Embryonic and adult-derived resident cardiac macrophages are maintained through distinct mechanisms at steady state and during inflammation. Immunity 2014;40:91–104.

58. Toldo S, Mezzaroma E, O'Brien L, et al. Interleukin-18 mediates interleukin-1–induced cardiac dysfunction. Am J Physiol Heart Circ Physiol 2014;306:H1025–31.

KEY WORDS exosome, FoxO3a, miR-155, pyroptosis, uremic cardiomyopathy

APPENDIX For supplemental tables and figures, please see the online version of this paper.